# Monophosphate Tungsten Bronzes with Hexagonal Tunnels, $Na_x(PO_2)_4(WO_3)_{2m}$: X-ray Diffraction and HREM Study

By B. Domengès, M. Hervieu and B. Raveau

*Laboratoire de Cristallographie et Sciences des Matériaux, ISMRA, boulevard du Maréchal Juin, 14032 Caen CEDEX, France*

## Abstract

An extensive study of the $MPTB_H$ family, $Na_x(PO_2)_4(WO_3)_{2m}$, by high-resolution electron microscopy and X-ray diffraction is reported. Non-stoichiometric defects, irregular intergrowths, domains, extra hexagonal tunnel rows, extra pentagonal tunnel rows and variations of the sodium content in the hexagonal tunnels are observed. Comparisons are made with the $MPTB_H$ family in which Na is replaced by K. This allows a further evaluation of cation (K and Na) influence on these compounds.

## Introduction

Phosphate tungsten bronzes (PTB's) form an original family of mixed-valence compounds whose framework results from the association of covalent 'phosphate layers' with a metallic $ReO_3$-type matrix. In these oxides, the phosphate layers are built up from $PO_4$ tetrahedra (monophosphates, MPTB's) or $P_2O_7$ groups (diphosphates, DPTB's) corner-sharing with the $WO_6$ octahedra of the $ReO_3$-type slabs. The relative orientation of both the phosphate groups and the $WO_6$ polyhedra results in either hexagonal tunnels ($DPTB_H$'s and $MPTB_H$'s) or pentagonal tunnels ($DPTB_P$'s and $MPTB_P$'s). The hexagonal tunnels are fully or partly occupied by $A$ ions ($A$ = K, Rb, Ba, Na) (Benmoussa, Groult, Labbé & Raveau, 1984; Domengès, Goreaud, Labbé & Raveau, 1983; Giroult, Goreaud, Labbé & Raveau, 1980, 1981, 1982a,b, 1983; Labbé, Ouachée, Goreaud & Raveau, 1983; Lamire, Labbé, Goreaud & Raveau, 1987a,b). These materials offer an extraordinary profusion of non-stoichiometric phenomena which depend on numerous chemical and physical factors that are not yet completely understood. Their understanding requires a thorough examination of numerous samples, especially by electron microscopy. Such work undertaken in recent years has shown the existence of different non-stoichiometric mechanisms in MPTB's compared with DPTB's. Moreover, evidence of structural differences between $K-MPTB_H$'s and $Na-MPTB_H$'s has been provided by X-ray dif-

fraction studies (Benmoussa *et al.*, 1984; Domengès *et al.*, 1983; Lamire *et al.*, 1987a). Nevertheless, the number of sodium monophosphate bronzes which have been studied up to now is too small to draw conclusions about the different behavior of sodium and potassium in these phases. This paper deals with an electron microscopy investigation of the family $Na_x(PO_2)_4(WO_3)_{2m}$ ($2 \le m \le 20$); its structural behavior is compared with that of the $K-MPTB_H$'s (Domengès, Hervieu, Raveau & O'Keeffe 1988).

## Experimental

The $Na-MPTB_H$'s were prepared according to the usual method (Benmoussa *et al.*, 1984; Lamire *et al.*, 1987a). Mixtures of $Na_2CO_3$, $(NH_4)_2HPO_4$ and $WO_3$ were first heated in air at 873 K, in order to decompose carbonate and phosphate. Then adequate amounts of metallic tungsten where added and the homogeneous mixtures heated in evacuated silica ampoules at temperatures close to 1273 K for several days.

All samples were analyzed by X-ray diffraction using a Guinier–de Wolf camera and pure compounds were studied with a powder diffractometer (Philips) using Cu $K\alpha$ radiation. The electron microscopy study was performed on two different microscopes: a JEM 120CX (operating at 120 kV) and a JEM 200CX (200 kV). Both, when used for high-resolution work, were equipped with a top-entry goniometer ($\pm 10°$) and an objective lens with a spherical aberration constant $C_s = 0.8$ mm (0.7 mm in the 120CX). Lattice images were computed by use of the multislice method (O'Keeffe, Buseck & Iijima, 1978).

## X-ray results and structural recalls

Previous X-ray investigations have shown that $Na_x(PO_2)_4(WO_3)_{12}$ can be obtained as a pure phase for $1.1 \le x \le 4$ (Benmoussa *et al.*, 1984). Thus, besides studying the series $Na_2(PO_2)_4(WO_3)_{2m}$ as a function of $m$ ($m$ being integer and semi-integer), several samples with different $x$ values ($1 \le x \le 4$)

were synthesized. The resultant products do not seem to depend highly on the sodium content $x$, and the homogeneity range of the Na-MPTB$_H$ family appears wider ($1 \leq x \leq 4$) than that of the K-MPTB$_H$'s ($1.75 < x \leq 3$). For $m \leq 10$, four new pure phases have been stabilized in addition to the $m = 4$, 6, 7 members (Benmoussa *et al.*, 1984; Lamire *et al.*, 1987*a*). They correspond to the members $m = 5$, 8, 9 and 10. For $m > 10$, in contrast to the potassium compounds (Domengès *et al.*, 1988), mixtures were obtained which contain mostly MPTB$_H$'s, sometimes with some additional perovskite bronzes Na$_x$WO$_3$ (Réau, Fouassier, Leflem, Barraud, Doumerc & Hagenmüller, 1968; Ribnick, Post & Banks, 1963). The major phase corresponds to the members $m = 10$ and 12, but some isolated crystals with $m = 11$ and 13 have been identifed by electron diffraction.

The Na-MPTB$_H$ compounds crystallize with a monoclinic cell (Fig. 1) for which theoretical parameters can be easily deduced from the ReO$_3$-like sub-cell, in a similar way to the K-MPTB$_H$'s (Domengès *et al.*, 1988). The MPTB$_H$ framework is built up from ReO$_3$-like slabs joined through PO$_4$ planes, leading to the formation of hexagonal tunnels where the alkaline ions are located (Fig. 1). In the chemical formula Na$_x$(PO$_2$)$_4$(WO$_3$)$_{2m}$, $m$ corresponds to the number of WO$_6$ octahedra along the $[011]_{ReO_3}$ direction, giving the ReO$_3$-like slab width. The parameters of pure phases have been deduced from the X-ray diffractograms, and are in agreement with the theoretical values (Table 1). The X-ray diffraction studies of single crystals for the members $m = 4$, 6 and 7 show that, in the sodium compounds, the ReO$_3$-type slabs are corrugated and do not correspond to each other through the same symmetry element as in the isotype structure with potassium. This leads to a different cell and space group to those found in the potassium compounds; two consecutive ReO$_3$-like slabs form the cell of even-$m$ members, where the crystals show the systematic extinctions $h0l$ $l = 2n + 1$, $0k0$ $k = 2n + 1$, in agreement with space group $P2_1/c$. Sodium odd-$m$ members show the same cell (within about an $a$ translation) and space group
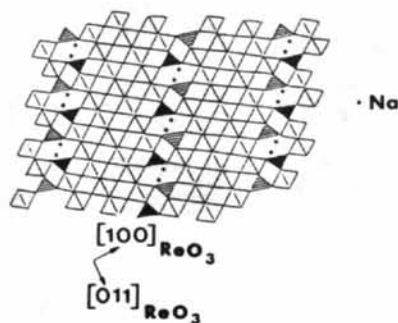
Table 1. Na$_2$(PO$_2$)$_4$(WO$_3$)$_{2m}$, Na-MPTB$_H$, *crystallographic data*

| $m$ | $a^*$ (nm) | $b^*$ (nm) | $c$ (nm) | $\beta$ (°) | $c_{th}$ (nm) | $\beta_{th}$ (°) |
|---|---|---|---|---|---|---|
| 4† | 0·6607 (5) | 0·5277 (4) | 1·779 (1) | 99·64 (5) | 1·75 | 99·5 |
| 5 | 0·6696 (4) | 0·5338 (3) | 2·110 (1) | 106·31 (5) | 2·12 | 106·1 |
| 6 | 0·6605 (2) | 0·5276 (2) | 2·362 (1) | 93·57 (3) | 2·36 | 93·7 |
| 7 | 0·6599 (2) | 0·5287 (2) | 2·706 (1) | 97·23 (5) | 2·69 | 97·9 |
| 8 | 0·6625 (4) | 0·5291 (2) | 3·022 (2) | 101·31 (4) | 3·03 | 101·2 |
| 9 | 0·6569 (3) | 0·5294 (2) | 3·313 (1) | 92·09 (5) | 3·28 | 92·5 |
| 10 | 0·6623 (3) | 0·5301 (2) | 3·623 (1) | 94·33 (3) | 3·61 | 95·7 |

\* Theoretical parameters of a member of the family Na$_x$(PO$_2$)$_4$(WO$_3$)$_{2m}$ are: $a_{th} = 0.66$, $b_{th} = 0.53$ nm.

† $x = 1.4$, data taken from Benmoussa *et al.* (1984).

($A2/m$, systematic extinction $hkl$ $k + l = 2n + 1$) as the analogous potassium compound. The $A2/m$ space group, with a mirror plane perpendicular to the $b$ axis, does not allow corrugated ReO$_3$-like slabs to be described. In fact, an X-ray study of the single crystal Na$_{1.7}$(PO$_2$)$_4$(WO$_3$)$_{14}$ (Lamire *et al.*, 1987*b*) showed that its structure is triclinic but the atomic positions, defined in the multiple cell deduced from the monoclinic one by a simple distortion [$a = 0.6575$ (2), $b = 0.5304$ (1), $c = 2.7076$ (3) nm, $\alpha = 89.62$ (1), $\beta = 96.17$ (1), $\gamma = 90.26$ (1)°], still obey the lattice translation $(b + c)/2$ leading to space group $A1$.

### Electron diffraction study

Based on these structural considerations, it appears that, in the reciprocal cell associated with the multi-
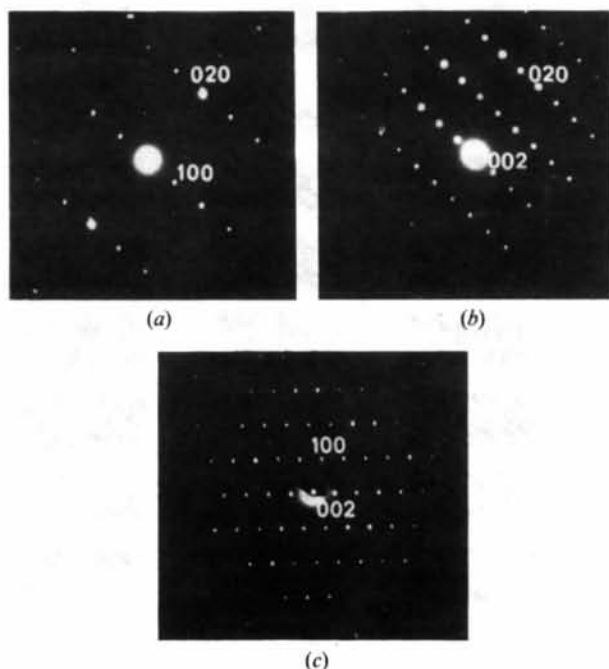
(a)    (b)

(c)

Fig. 2. Electron diffraction patterns of the $m = 5$ member showing the existence conditions (a) $hk0$ $k = 2n$, (b) $0kl$, $k + l = 2n$ and (c) $h0l$ $l = 2n$.

Fig. 1. Idealized (010) projection of Na$_x$(PO$_2$)$_4$(WO$_3$)$_{14}$.

ple real cell, the systematic extinctions are $hkl\ k + l = 2n + 1$ and that the triclinic symmetry may not be detected from the electron diffraction pattern if the distortion is too small (especially if its amplitude depends on the sodium content). Convergent-beam electron diffraction patterns would attest this loss of monoclinic symmetry (mirror plane perpendicular to $b$) but our classical electron diffraction results only confirm the lattice translation $(b + c)/2$ for all crystals corresponding to odd-$m$ members of the family as shown from Fig. 2.
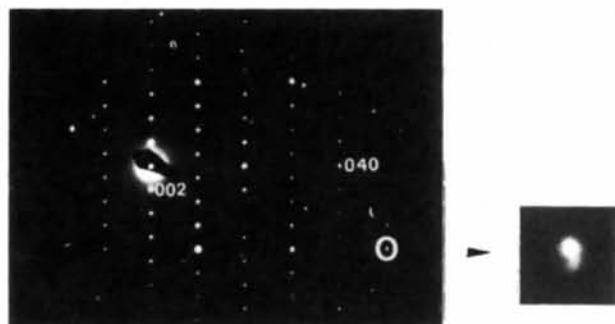


Fig. 3. (100) electron diffraction pattern showing the splitting of spots with high $k$ values (see enlargement of the circled spot).

Some crystals showed a triclinic distortion, but it could not be definitely related to the triclinic symmetry of the single crystals. Indeed, the observation of split spots, particularly $0k0$ reflections (Fig. 3), may suggest a triclinic distortion with the classical twinning phenomenon. However, as the amplitude of the splitting varies from one reciprocal plane to another in the same crystal, this observation will be interpreted here in terms of the coexistence of several domains in the crystal slightly disoriented from each other. Moreover, even-$m$-member crystals sometimes show this type of diffraction pattern and strain. Only the $m = 5$ crystals show, nearly systematically, a loss of the monoclinic symmetry. Generally, their electron diffraction patterns are characterized by a lattice of bright spots which follow the extinction condition $hkl\ k + l = 2n + 1$ and by split reflections which confirm the triclinic distortion and the twinning phenomenon.

## HREM study

The HREM study of the Na-MPTB$_H$'s was carried out initially on regular members to allow the interpretation of the experimental images using image

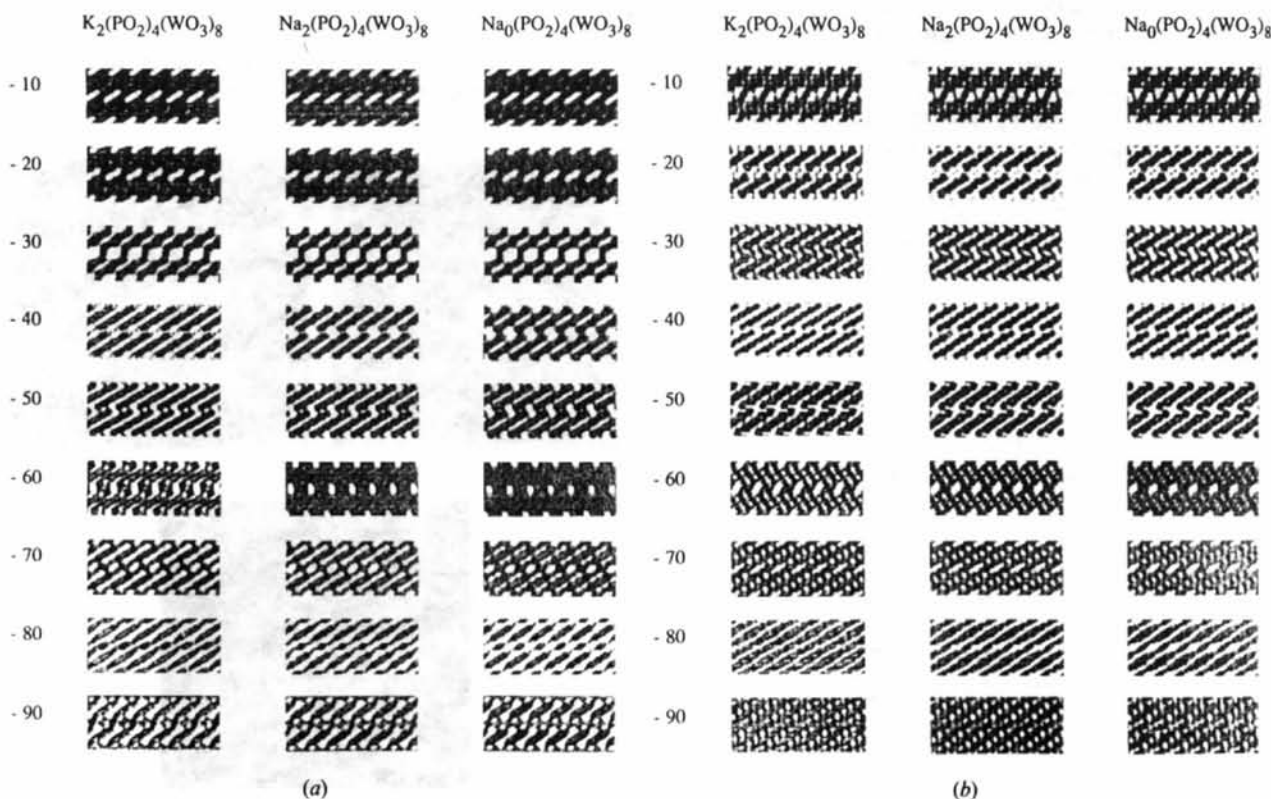

(a)                                                    (b)

Fig. 4. (010) calculated through-focus series for (a) JEM 120CX and (b) JEM 200CX microscopes. Calculation parameters are: crystal thickness $T = 3\cdot2$ nm; (a) high-voltage $V = 120$ kV, spherical aberration constant $C_s = 0\cdot7$ mm, convergence half-angle $\alpha/2 = 0\cdot65$ mrad, focus spread $\Delta/2 = 10$ nm, 33 beams in the objective aperature; (b) $V = 200$ kV, $C_s = 0\cdot8$ mm, $\alpha/2 = 0\cdot8$ mrad, $\Delta/2 = 7\cdot5$ nm, 137 beams in the objective aperture; defocus values are given in nanometers.

computations derived from the X-ray structural data of $Na_{1.5}(PO_2)_4(WO_3)_8$ (Benmoussa, *et al.* 1984). Two effects special to Na-MPTB$_H$ can influence the contrast: sodium instead of potassium in the hexagonal tunnels and corrugation of the ReO$_3$-like slabs. To allow comparison of both of these effects, calculations were performed for both families, K- and Na-MPTB$_H$'s, on the same member $m = 4$ (Benmoussa *et al.*, 1984; Domengès *et al.*, 1983; Lamire *et al.*, 1987*a,b*) and with a sodium cation content $x = 2$. For a thickness of 3 nm, and irrespective of the microscope used (JEM 200CX and JEM 120CX), calculated through-focus series show an almost identical contrast for both families (Fig. 4). The main difference is in the contrast of the hexagonal tunnels on the images where the tunnels are enhanced, *i.e.* between 20 and 30 nm for JEM 200CX and 40 and 50 nm for JEM 120CX. On these images, the difference in mass between sodium and potassium results in a slight difference of shape in the imaging of the hexagonal tunnels. Nevertheless, images can be directly compared. Samples of $Na_x(PO_2)_4$-$(WO_3)_{2m}$, with $x = 2$ and $m$ an integer ranging from 4 to 10, were studied. Some preparations with $x = 1.3$ and 3 were also investigated. From this study, most crystals appear as regular, except in samples of nominal composition $m = 5$.

*Regular crystals*

At the optimum defocus, the (010) images of the thin edges of the crystals show a direct projection of the structure potential. An example is given in Fig. 5 for an $m = 10$ crystal. Thus in the WO$_3$ slabs, the rectangular lattice of spots, $0.38 \times 0.27$ nm$^2$, can be associated with the perovskite-type tunnels: along the $[011]_{ReO_3}$ direction, nine spots are observed, correlated with the nine perovskite-type tunnels formed by the ten octahedra of the ReO$_3$-like slabs. Between them, large spots, with a 'nut' shape, alternate with single spots. They correspond to the hexagonal and rhombic tunnels of the structure, respectively (Fig. 5*b*). The nut shape of the spot corresponding to the hexagonal tunnels is due to the presence of the cations; the same feature is observed in the K-MPTB$_H$'s, but enhanced with spots corresponding to hexagonal tunnels split into two. This dependence of the contrast on the cation content appears clearly on calculated images for both K-MPTB$_H$'s (Domengès
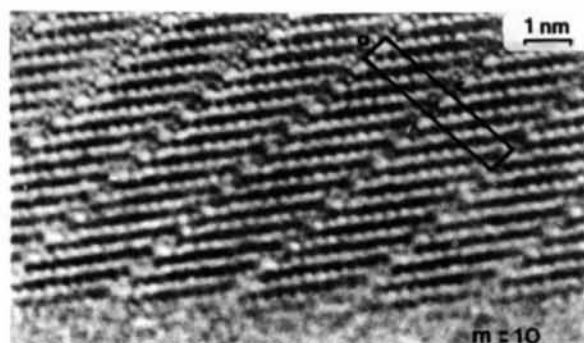


(*a*)
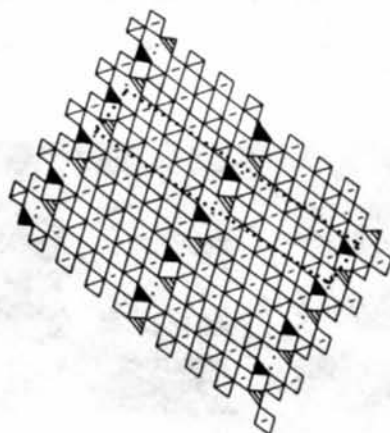


(*b*)

Fig. 5. (*a*) (010) high-resolution image of an $m = 10$ crystal (JEM 200CX). At this defocus value, spots are related to the tunnels of the structure: hexagonal, rhombic and perovskite-type. (*b*) Idealized (010) projection of the $Na_x(PO_2)_4(WO_3)_{20}$ structure.
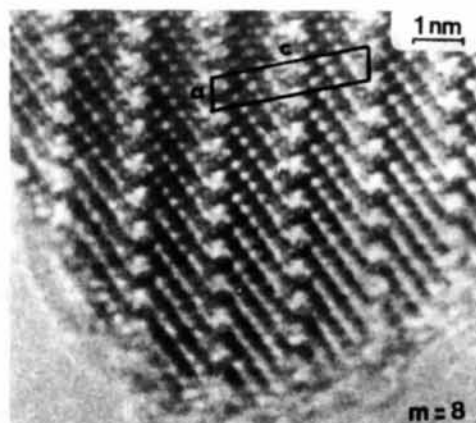


Fig. 6. (010) high-resolution images of $m = 8$ and $m = 5$ crystals (JEM 200CX).

et al., 1988) and Na-MPTB$_H$'s (Fig. 4). Through these HREM images, identification of any member of the series can be made directly by counting the number of perovskite-type tunnels. Two examples are given in Fig. 6 for $m = 5$ and $m = 8$ regular crystals, where four and seven spots are observed, respectively.

### Observation of defects

The observed defects in the Na-MPTB$_H$'s can be classified into two groups which deal with (i) the distribution of the phosphate planes with respect to the ReO$_3$-type slabs, and (ii) the distribution of the PO$_4$ groups in the phosphate planes.

(i) *The distribution of the phosphate planes with respect to the ReO$_3$-type slabs. Irregular intergrowth.* Besides the nearly perfect crystals, some appear very disordered. Their electron diffraction patterns usually show diffuse streaks parallel to the reciprocal c axis and images show irregular sequences of different members of the family (Fig. 7). This phenomenon occurs very frequently in the sample corresponding to $m = 5$ and for high values of $m$ ($m > 12$). The latter result is not surprising as members higher than 13 could not be synthesized as regular microcrystals and the $m = 5$ member shows unusual behavior for the phosphate bronzes (Domengès *et al.*, 1983; Benmoussa, Labbé, Groult & Raveau, 1982; Domengès, Hervieu & Raveau, 1984; Domengès, Hervieu, Tilley & Raveau, 1984). Classically, the defective slabs always correspond to a number of octahedra close to that of the matrix. When two

members are prevalent in a crystal, their corresponding reciprocal lattices are superimposed on the electron diffraction pattern and images show sequences of both members, usually irregular. An example of a microcrystal selected in an $m = 8$ nominal matrix is shown in Fig. 8, where a sequence of $m = 7$ and $m = 8$ members is observed, which are almost regularly intergrown. The high-$m$ members often exhibit defective $m'$ slabs. Such behavior is typical of structures whose building principle is the intergrowth of two different structural units and has been observed in phosphate bronzes (Domengès *et al.*, 1983; Domengès, Hervieu & Raveau, 1984; Hervieu & Raveau, 1983a,b) and other bronzes such as crystallographic shear phases (Blomberg, Khilborg & Magnéli, 1953; Magnéli, 1953) or intergrowth tungsten bronzes (ITB's) (Hussain & Khilborg, 1976; Khilborg, 1978).

*Domains.* Another type of defect is observed in the Na-MPTB$_H$ crystals, corresponding to growth accidents; two different structural features are responsible:

(1) A stepping growth: this involves small domains of different thickness on the crystal edges. These domains are sometimes slightly misoriented with
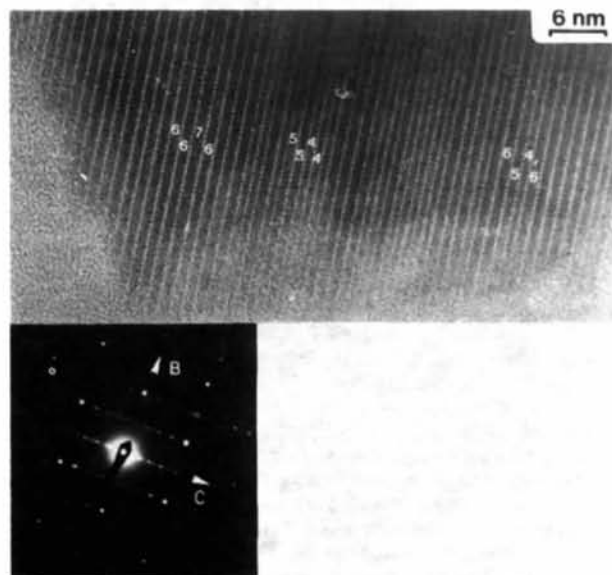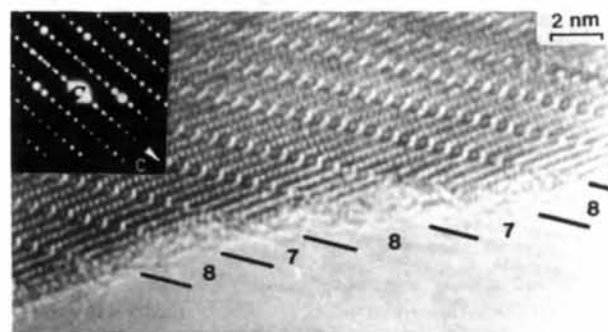


Fig. 8. (010) electron diffraction pattern and high-resolution image of a crystal selected from an $m = 8$ preparation. The almost regular intergrowth of the $m = 7$ and $m = 8$ members is shown (JEM 200CX).



Fig. 7. (100) electron diffraction pattern and high-resolution image of a crystal selected from an $m = 5$ preparation. The width of the ReO$_3$-type slabs varies from 4 to 7 (JEM 200CX).
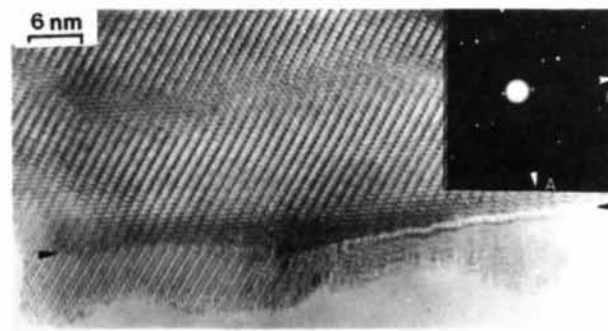


Fig. 9. (010) electron diffraction pattern and high-resolution image of an $m = 6$ crystal. Crystal growth has stopped and begun again leading to the formation of amorphous and crystallized zones, much thinner than the parent crystal (JEM 120CX).

regard to the bulk and sometimes poorly-crystallized or amorphous. An example of such a crystal selected in an $m = 6$ matrix is shown Fig. 9. Crystal growth has stopped and then begun again leading to the formation on the crystal edge of an amorphous domain and a crystallized one, much thinner than the parent crystal. The constrast varies strongly from one side of the step to the other and tunnel rows seem to shift at the step, but geometrical measurements show that tunnel rows of the thin 'outgrowth' are perfectly aligned with those of the matrix. The step between crystal and amorphous domains appears 'steep' and as a clear edge.

(2) A mechanism of oriented domains: this involves the division of the crystals into two large parts. The corresponding crystals are characterized by an electron diffraction pattern typical of the superimposition of two disoriented lattices (Fig. 10). Selected-area electron diffraction patterns allow the isolation of two $m = 6$ domains in which the $b$ axes are nearly parallel. The low-resolution image shows a microcrystal divided into two parts, with a domain boundary wandering through, along a mean direction inclined at 45° towards the fringes of each area, the fringes being associated with the hexagonal tunnel rows or phosphate planes of the structure (Fig. 11). In the bulk, fringe brightness varies sometimes. As shown by the fringe spacing on enlargements of the crystal edge, the fringes correspond to thinner $ReO_3$-type slabs than most of those of the $m = 6$ matrix. Details of the boundary allow us to propose a model of the junction between both domains through a coherent boundary. A careful geometrical analysis leads to a model using $PO_4$ tetrahedra, staggered $P_2O_7$ groups, similar to those
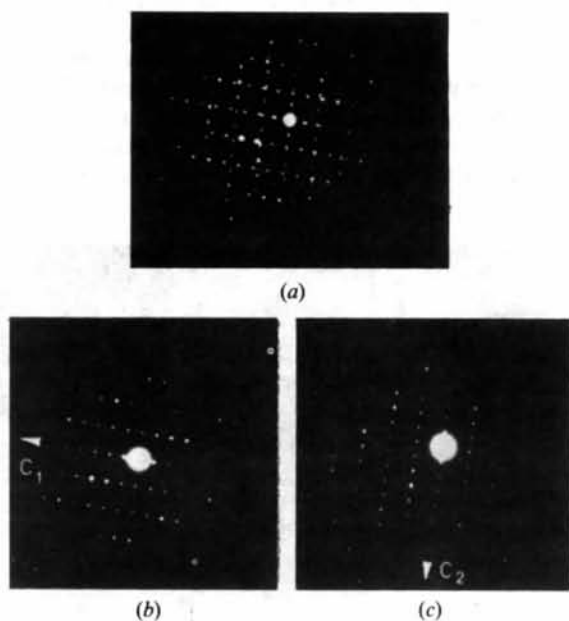


(a)



(b)                                    (c)

Fig. 10. (a) Electron diffraction pattern showing the superimposition of two $h0l$ lattices. (b), (c) Selected-area electron diffraction patterns of each lattice which correspond to an $m = 6$ member and share the same $b$ axis.



(a)



Fig. 11. Low-resolution image corresponding to Fig. 10 showing two domains. Bright fringes are associated with $ReO_3$-type slabs of a different width from those of the matrix.
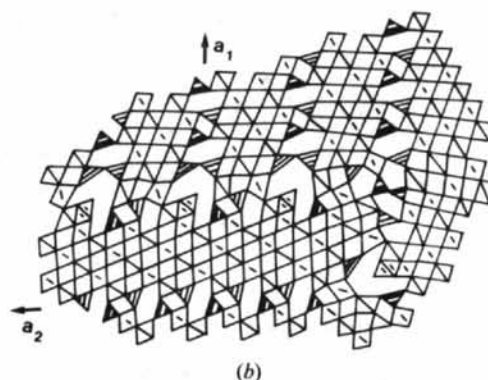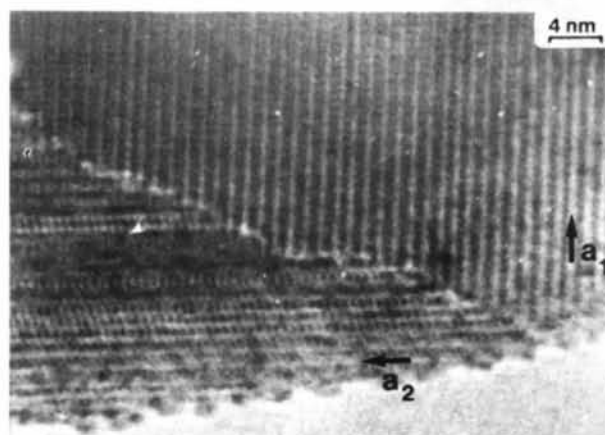


(b)

Fig. 12. (a) Detail of Fig. 11 showing the coherent boundary between both domains. (b) Idealized projection of a model for the structure of the boundary based on $PO_4$, $P_2O_7$ groups and sheared $WO_6$ octahedra.

of $P_8W_{12}O_{52}$ structure (Domengès, Goreaud, Labbé & Raveau, 1982), and edge-sharing $WO_6$ octahedra, which lower the number of unshared O atoms (Fig. 12). The boundary is roughly parallel to the hexagonal tunnel rows and wanders in the crystal step by step. The proposed model fits the observations satisfactorily but can certainly not be considered as unique. Nevertheless, its constituent elements,

$PO_4$, $P_2O_7$ groups and sheared octahedra, probably appear throughout the boundary.

(ii) *The distribution of the $PO_4$ groups in the phosphate planes.* The easy inversion of $PO_4$ tetrahedra and $WO_6$ octahedra results in two types of defects.

*Extra hexagonal tunnel rows.* As mentioned previously, crystals exhibiting perovskite slabs as large as 13 octahedra are easily observed in high-$m$-value members; some of them are very regular, others are disordered and correspond to irregular intergrowths of members ranging from $m = 10$ to $m = 13$. In the larger slabs, unusual contrast is often observed as shown in Fig. 13: the crystal, selected in an $Na_2(PO_2)_4(WO_3)_{24}$ sample ($m = 12$), is characterized by an electron diffraction pattern typical of the superimposition of several members higher than 10 and the corresponding image shows irregular intergrowth. The contrast observed in some slabs among the widest ($m = 13$) can be interpreted by the formation of hexagonal tunnel rows, *i.e.* phosphate planes (Fig. 13), similar to the defective slabs observed in the $MPTB_P$'s (Domengès, Hervieu, Tilley
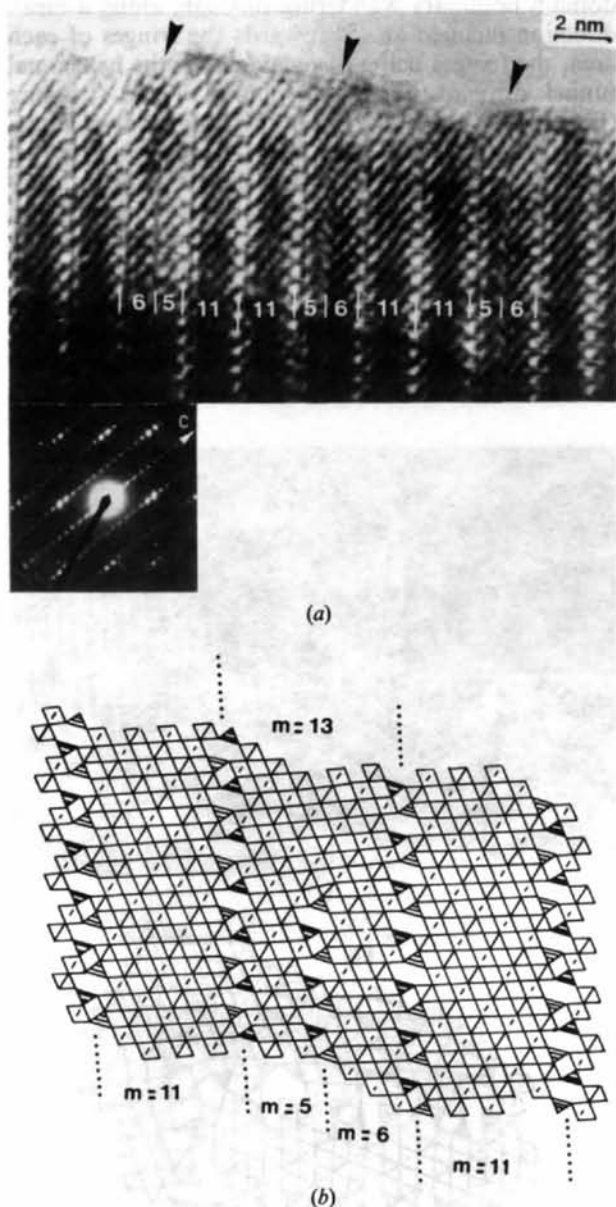


(a)



(b)

Fig. 13. (a) (010) electron diffraction pattern and high-resolution image of a crystal selected in an $m = 12$ preparation. The electron diffraction pattern shows the superimposition of two terms $m = 11$ and 12. Defects appear in the widest ($m = 13$) $ReO_3$-type slabs of the crystal (arrowed), which are associated with extra hexagonal tunnel rows (JEM 120CX). (b) Idealized projection of the proposed model.
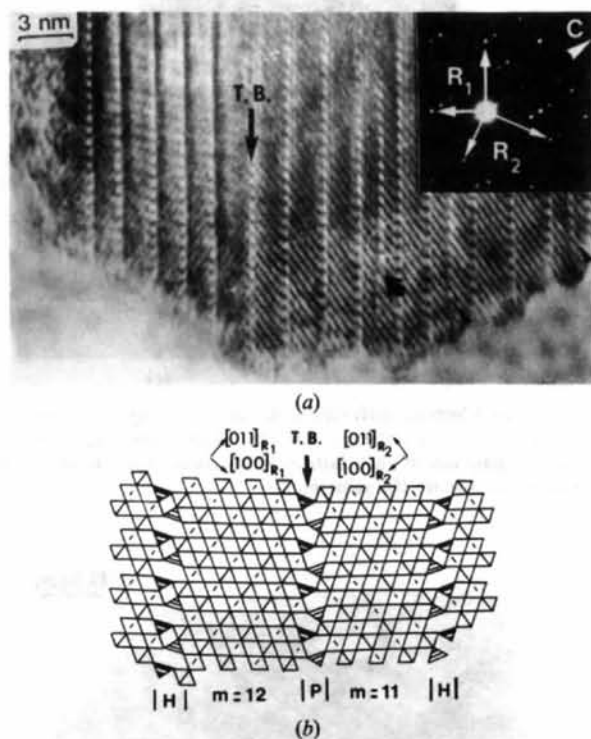


(a)



(b)

Fig. 14. (a) Electron diffraction pattern and medium-resolution image of a crystal selected in an $m = 20$ preparation. The electron diffraction pattern shows the superimposition of two $h0l$ twinning $MPTB_H$ lattices. In the medium-resolution image, the twin boundary (T.B.) shows a typical contrast of the phosphate planes in the $MPTB_P$. On the right-hand side of the image, extra hexagonal tunnel rows (arrowed) appear in the wide $ReO_3$-type slabs ($m = 13$ and 15) and another row shifts (curved arrow) (JEM 120CX). (b) Idealized projection of a model of the twin boundary structure.

& Raveau, 1984). These extra rows stop in the $ReO_3$-type slab, by replacement of two $PO_4$ groups by two $WO_6$ octahedra. The contrast of the extra hexagonal tunnels is slightly different from that of the matrix because of the accommodation of the defect by the neighboring framework. Of course, the sodium content in these extra tunnels cannot be given accurately. This defect has been encountered in slabs corresponding to an $m$ value higher than 13 octahedra and smaller than 15. When these extra rows are not stopped in the crystals, they result in the appearance of two adjacent low-$m$-value slabs in a matrix of large slabs. This type of defect is not encountered in the K-$MPTB_H$'s, as no member larger than $m = 10$ is stabilized.

*Extra pentagonal tunnel rows.* In an $Na_3(PO_2)_4$-$(WO_3)_{40}$ preparation ($m = 20$), a selected crystal showed an electron diffraction pattern similar to that of a disordered $MPTB_P$ crystal (Fig. 14). But a difference in intensity of the strong spots of the $ReO_3$ sublattice suggests the existence of a twin, the twin boundary being parallel to the (001) plane. The corresponding medium-resolution image confirms this interpretation. Between the rows of brighter spots (*i.e.* hexagonal tunnel rows), the gray lines are associated with perovskite-type tunnels and give the direction of the octahedral chains in the $ReO_3$-type slabs. An interesting feature is observed: the direction of the octahedral chains changes from the left to the right part of the crystal; both chains are oriented at 70°. Thus, the crystal consists of two twinning $MPTB_H$ domains sharing the (001) plane. This geometrical relation and the contrast at the twin boundary leads to the following model, based on two $MPTB_H$ domains joined through a double plane of $PO_4$ tetrahedra forming pentagonal tunnels, as in the

$MPTB_p$'s (Fig. 14b). This crystal can thus be symbolized by the sequence: |H|9|H|11|H|9|H|9|H|12|P|11|H|12|H|11|H|... where H and P symbolize hexagonal and pentagonal tunnel rows respectively, and the numbers correspond to the number of octahedra in the $ReO_3$-type slabs, *i.e.* the $m$ value. Note on the right-hand side of the crystal three defects corresponding to three broken extra rows of hexagonal tunnels (arrowed) and especially the shifting of one of these extra rows (curved arrow).
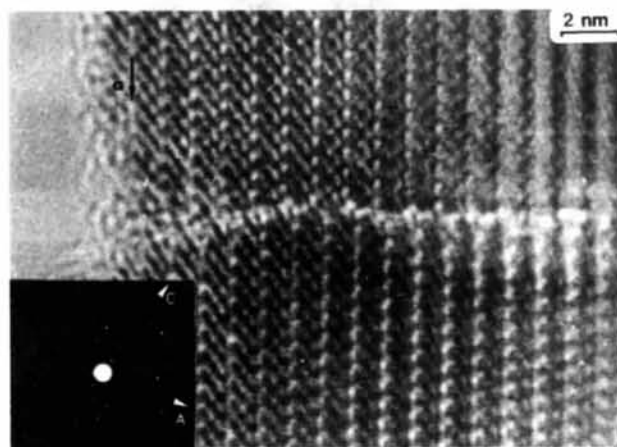




Fig. 15. Electron diffraction pattern and high-resolution image of an $m = 5$ crystal. Twelve successive hexagonal tunnel rows shift on the edge of the crystal without straining the neighboring framework.

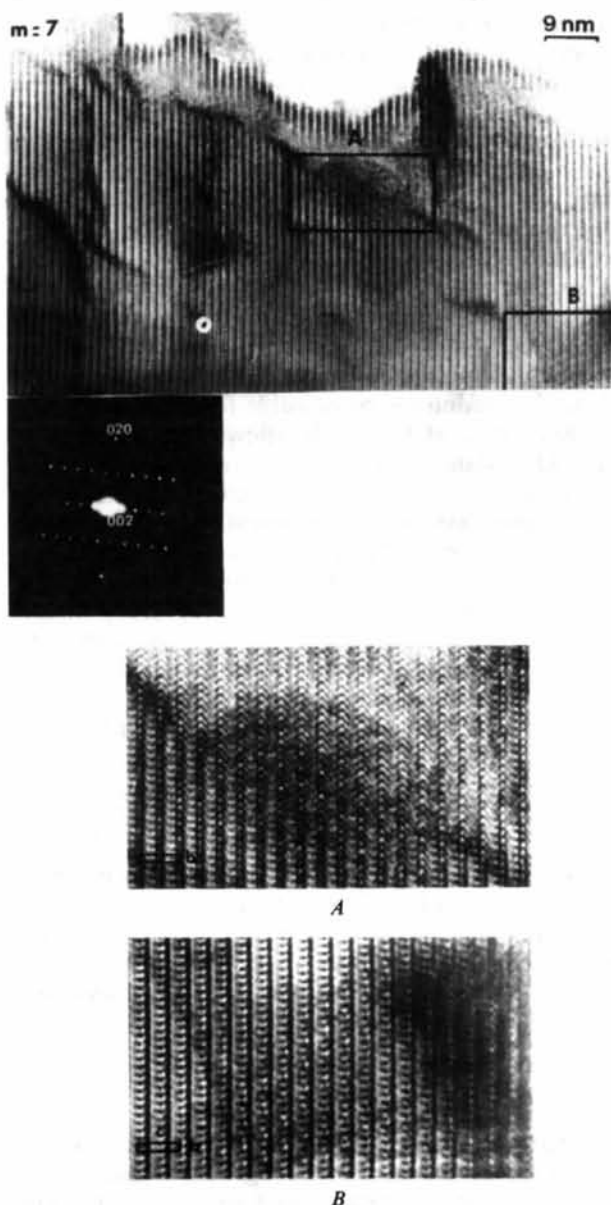

Fig. 16. (100) electron diffraction pattern and high-resolution image of an $m = 7$ crystal selected in an $Na_3(PO_2)_4(WO_3)_{14}$ preparation. Dark stripes appear throughout the crystal and Moiré patterns introduce a new local periodicity in areas $A$ and $B$ (JEM 120CX).

*Antiphase boundaries.* This type of defect is rarely observed; an example is shown in Fig. 15. A very regular $m = 5$ crystal shows on its edge an anomalous contrast typical of a shift. Nearly 12 successive hexagonal tunnel rows are shifted perpendicularly to $a$, the neighboring framework being unaffected on each side of the defect. The periodicity stays perfectly equal to $m = 5$ and the defect is accommodated in the bulk of the crystal.

(iii) *Distribution of* Na$^+$ *in the tunnels.* The following example can be considered as unique. In an Na$_3$(PO$_2$)$_4$(WO$_3$)$_{14}$ preparation $(m = 7)$, the [100] high-resolution image of a selected crystal shows, despite a perfect electron diffraction pattern (no triclinic distortion and existence conditions $0kl$, $k + l = 2n$), dark contrast stripes often parallel to the [010] direction (Fig. 16). Details enhance two points: first, the $c$ direction varies slightly from one side of the dark stripes to the other; second, some area constrast suggests the presence of a new periodicity, but very localized. By analogy with K-MPTB$_H$ observations, these phenomena may be due to local ordering of Na$^+$ content, which would introduce strains on the framework by local variations in the cell volume. Indeed, X-ray studies on Na-MPTB$_H$ single crystals show that sodium is responsible for the corrugation of ReO$_3$-type slabs which allows the lowering of Na—O distances and ensures a quasi-tetrahedral environment of Na$^+$ in the hexagonal tunnels. Image calculations have been performed with the observation conditions, and characteristic results are shown in Fig. 17. The variation of sodium content cannot, alone, influence the contrast of the [100] images relative to the [010] ones. Thus, it appears that the preceding observation reflects strains on the matrix of the selected crystal probably due to the local distortions of the hexagonal tunnels related to variation of sodium content, in a similar way to the O-deficient perovskite Ba$MO_{3-x}$ (Hutchison & Jacobson, 1977; Caignaert, Hervieu, Domengès, Nguyen, Pannetier & Raveau, 1988). This phenomenon is unique in the Na-MPTB$_H$ series as no other case of significant variation of Na$^+$ content has been detected, either by direct observation of the contrast or by extra superstructure spots in the electron diffraction patterns, irrespective of the observation direction, [100] or [010].

## Concluding remarks

The nature of the cation in the hexagonal tunnels also plays a role in the homogeneity range of the MPTB$_H$ phases as well as in their inner structure. Several differences of behavior between Na-MPTB$_H$'s and K-MPTB$_H$'s have been encountered:

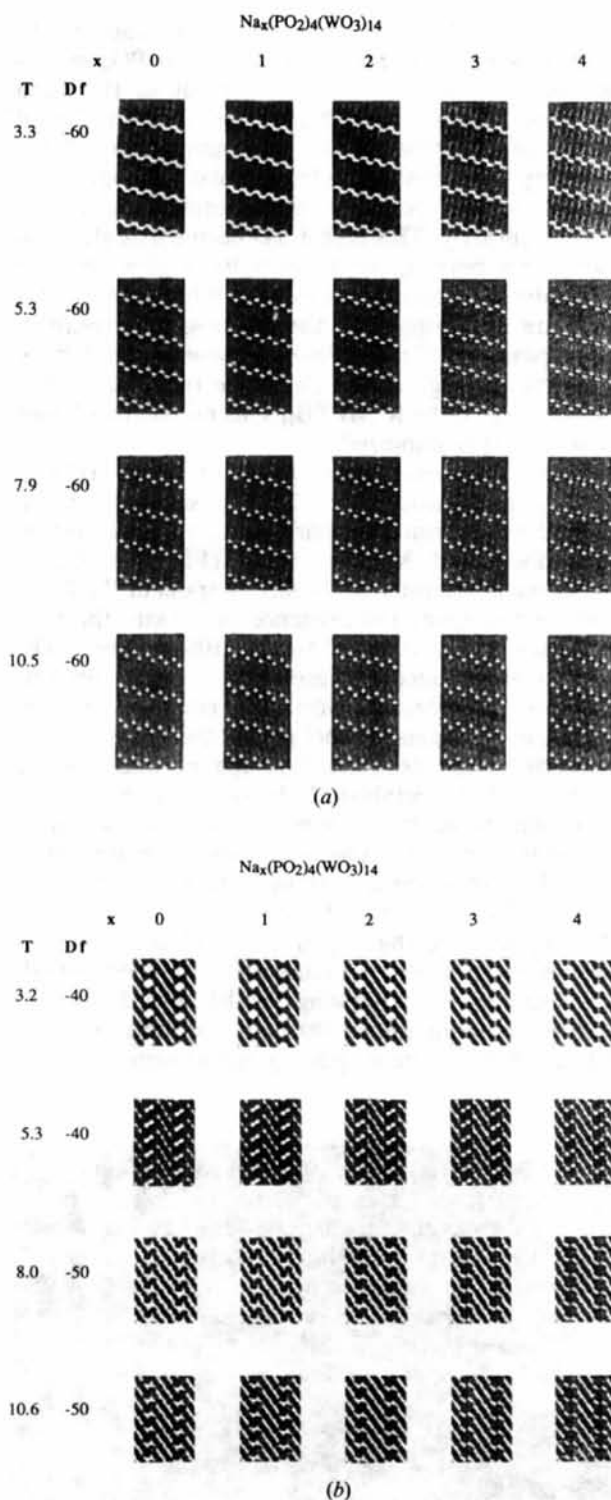(1) The ReO$_3$-type slabs are corrugated in the whole Na-MPTB$_H$ family.



(a)



(b)

Fig. 17. Characteristic calculated images for several sodium contents $x$ and thicknesses $T$. Calculations parameters are: high voltage $V = 120$ kV, spherical aberration constant $C_s = 0.7$ mm, half-divergence angle $\alpha/2 = 0.6$ mrad, focus spread $\Delta/2 = 10$ nm; (a) (100) projection, 91 beams in the objective aperture; (b) (010) projection, 49 beams in the objective aperture. Thicknesses $T$ and defocus values Df are in nanometers.

(2) The $m = 5$ member has been stabilized for the first time, but crystals are usually affected by strains (triclinic distortion and frequent intergrowth defects). Possibly, the $m = 4$ and 6 members are favored in the K-MPTB$_H$'s because of their stability and the stiffness of the framework (higher order of symmetry).

(3) Higher members have been synthesized in Na-MPTB$_H$'s ($m \le 13$) than in K-MPTB$_H$'s ($m \le 10$). The reason may be that only two structural types of Na$_x$WO$_3$ phases are stabilized and with a wide homogeneity range: perosvskite tungsten bronzes ($x < 0\cdot11$ and $0\cdot41 < x < 0\cdot95$) and tetragonal tungsten bronzes ($0\cdot26 < x < 0\cdot38$), whereas three structural types of K$_x$WO$_3$ phases (intergrowth, hexagonal and tetragonal tungsten bronzes) are successively stabilized in the range $0\cdot06 < x < 0\cdot57$. But surprisingly, the width of the ReO$_3$-type slabs is still limited. In the case of sodium-deficient phases, the Na$_x$WO$_3$ PTB's are synthesized for $x < 0\cdot11$, i.e. Na/W $< 0\cdot11$. Considering the Na-MPTB$_H$ formulation, Na$_2$(PO$_2$)$_4$-(WO$_3$)$_{2m}$, this ratio is obtained for $m \ge 9$. Moreover, ReO$_3$-type slabs are corrugated so that the perovskite-type cages are very similar in both structures. There should be no limitation to the width of ReO$_3$-type slabs in the Na-MPTB$_H$'s. However, synthesis of higher members ($m \ge 10$) only leads to the formation of $m = 10$ and 12 crystals, sometimes 11 and 13, and most often hexagonal tunnel rows appear in the wider ReO$_3$-type slabs ($m \ge 13$) which give locally two thinner slabs.

(4) The adaptability of the Na-MPTB$_H$ framework compared with that of the K-MPTB$_H$'s allows more classical defects of the phosphate tungsten bronzes to be formed (especially the insertion of an extra hexagonal tunnel row in a ReO$_3$-type slab). In the same way, pentagonal tunnel rows have been observed, but isolated in an MPTB$_H$ matrix and not as an intergrowth of both structures as in the higher members of MPTB$_P$'s; this feature is probably related to the tunnel shape. Hexagonal tunnels, where the $A$ ions are located, can be stabilized without any inserted ions leading to intergrowth phases. By way of contrast, the presence of $A$ ions in the structure hinders the formation of pentagonal tunnels.

(5) Local ordering of the sodium in the hexagonal tunnels has been encountered only once in a sodium-rich preparation ($x = 3$). The smaller size of the sodium ion compared to that of potassium may favor a random distribution. Moreover, variations of sodium content introduce strains in the framework.

## References

BENMOUSSA, A., GROULT, D., LABBÉ, PH. & RAVEAU, B. (1984). *Acta Cryst.* C40, 573–576.

BENMOUSSA, A., LABBÉ, PH., GROULT, D. & RAVEAU, B. (1982). *J. Solid State Chem.* 44, 318–325.

BLOMBERG, B., KHILBORG, L. & MAGNÉLI, A. (1953). *Ark. Kemi*, 6(11), 133–137.

CAIGNAERT, V., HERVIEU, M., DOMENGÈS, B., NGUYEN, N., PANNETIER, J. & RAVEAU, B. (1988). *J. Solid State Chem.* 73, 107–117.

DOMENGÈS, B., GOREAUD, M., LABBÉ, PH. & RAVEAU, B. (1982). *Acta Cryst.* B38, 1724–1728.

DOMENGÈS, B., GOREAUD, M., LABBÉ, PH. & RAVEAU, B. (1983). *J. Solid State Chem.* 50, 173–179.

DOMENGÈS, B., HERVIEU, M. & RAVEAU, B. (1984). *Acta Cryst.* B40, 249–256.

DOMENGÈS, B., HERVIEU, M., RAVEAU, B. & O'KEEFFE, M. (1988). *J. Solid State Chem.* 72, 155–172.

DOMENGÈS, B., HERVIEU, M., TILLEY, R. J. D. & RAVEAU, B. (1984). *J. Solid State Chem.* 54, 10–28.

GIROULT, J. P., GOREAUD, M., LABBÉ, PH. & RAVEAU, B. (1980). *Acta Cryst.* B36, 2570–2575.

GIROULT, J. P., GOREAUD, M., LABBÉ, PH. & RAVEAU, B. (1981). *Acta Cryst.* B37, 1163–1166.

GIROULT, J. P., GOREAUD, M., LABBÉ, PH. & RAVEAU, B. (1982a). *Acta Cryst.* B38, 2342–2347.

GIROULT, J. P., GOREAUD, M., LABBÉ, PH. & RAVEAU, B. (1982b). *J. Solid State Chem.* 44, 407–414.

GIROULT, J. P., GOREAUD, M., LABBÉ, PH. & RAVEAU, B. (1983). *Rev. Chim. Minér.* 20, 829–836.

HERVIEU, M. & RAVEAU, B. (1983a). *Chem. Scr.* 22, 117–122.

HERVIEU, M. & RAVEAU, B. (1983b). *Chem. Scr.* 22, 123–128.

HUSSAIN, A. & KHILBORG, L. (1976). *Acta Cryst.* A32, 551–557.

HUTCHISON, J. L. & JACOBSON, A. J. (1977). *J. Solid State Chem.* 20, 417.

KHILBORG, L. (1978). *Chem. Scr.* 14, 187.

LABBÉ, PH., OUACHÉE, D., GOREAUD, M. & RAVEAU, B. (1983). *J. Solid State Chem.* 50, 163–172.

LAMIRE, M., LABBÉ, PH., GOREAUD, M. & RAVEAU, B. (1987a). *J. Solid State Chem.* 66, 64–72.

LAMIRE, M., LABBÉ, PH., GOREAUD, M. & RAVEAU, B. (1987b). *J. Solid State Chem.* 71, 342–348.

MAGNÉLI, A. (1953). *Acta Cryst.* 6, 495–500.

O'KEEFFE, M., BUSECK, P. R. & IIJIMA, S. (1978). *Nature (London)*, 234, 322–324.

RÉAU, J. M., FOUASSIER, C., LEFLEM, G., BARRAUD, J. Y., DOUMERC, J. P. & HAGENMÜLLER, P. (1968). *Rev. Chim. Minér.* 7, 966.

RIBNICK, A. S., POST, B. & BANKS, E. (1963). *Adv. Chem. Ser.* 39, 246.